Frontiers in Bioscience Landmark

Front. Biosci. (Landmark Ed) **2026**; 31(6): 51641
https://doi.org/10.31083/FBL51641

Original Research

Abnormal Polyamine Metabolism in Pancreatic Epithelial Cells aggravates chronic pancreatitis-associated preneoplastic lesions

Yuhong Zhang[1,2], Hongbin Wang[3], Xiaxia Shao[2], Yang Ling[4,*], Yongping Liu[5,6,*]

[1]Department of Oncology, The Third Affiliated Hospital of Soochow University (Changzhou Cancer Hospital), 213032 Changzhou, Jiangsu, China
[2]Department of Oncology, Affiliated Jiangyin Hospital of Nantong University, 214400 Jiangyin, Jiangsu, China
[3]Department of Emergency, Jiangyin Hospital Affiliated to Nanjing University of Chinese Medicine, 214400 Jiangyin, Jiangsu, China
[4]Department of Oncology, Changzhou Cancer Hospital, 213032 Changzhou, Jiangsu, China
[5]Clinical Oncology Laboratory, Changzhou Cancer Hospital, 213032 Changzhou, Jiangsu, China
[6]Medical Oncology Department, Changzhou Cancer Hospital, 213032 Changzhou, Jiangsu, China
*Correspondence: medilyn@vip.126.com (Yang Ling); liuyongping026@126.com (Yongping Liu)
Academic Editor: Sung Eun Kim
Submitted: 9 March 2026 Revised: 13 May 2026 Accepted: 22 May 2026 Published: 25 June 2026

Abstract

Background: Chronic pancreatitis (CP) is an independent risk factor for pancreatic cancer (PC). Investigation of the pathological progression of CP may help to elucidate the mechanisms underlying the progression of preneoplastic lesions in CP. **Methods**: Interleukin-6 (IL-6)and Tumor necrosis factor-alpha (TNF-α) were used to induce inflammatory mouse pancreatic acinar carcinoma cell line 83 (MPC-83) cells, followed by RNA-sequencing to identify differentially expressed genes. Quantitative real-time polymerase chain reaction (qRT-PCR) and Western blot were used to assess mRNA expression and protein levels, respectively. Flow cytometry was used to quantify CD86- and CD206-positive cells, and the Transwell assays were used to assess cell migration. Methylation-specific PCR (MSP-PCR) was used to assess DNA methylation, and enzyme-linked immunosorbent assay (ELISA) to measure Interferon-gamma (IFN-γ), IL-10, spermine, and spermidine levels. Hematoxylin-Eosin (HE) and Masson staining were used to assess pathological changes and collagen deposition in pancreatic tissues, and immunohistochemistry was used to detect alpha-smooth muscle actin (α-SMA), cluster of differentiation 86 (CD86), and cluster of differentiation 206 (CD206) expression. **Results**: Spermine and spermidine levels were elevated in inflammatory MPC-83 cells and the serum and pancreatic tissues of a CP mouse model, respectively. IL-6 and TNF-α increased the mRNA expression of Ornithine decarboxylase (*ODC*), Spermine synthase (*SMS*), and Spermidine synthase (*SRM*), and decreased Spermidine/spermine N1-acetyltransferase 1 (*SAT1*) mRNA expression. Spermine further increased the mRNA expression of SRY-box 9 (*SOX9*) and Keratin 19 (*KRT19*) in inflammatory MPC-83 cells and reduced the DNA methyltransferase 3b (DNMT3B) protein level. Spermine also reduced the methylation of *SOX9* and *KRT19* in MPC-83 cells. The enhanced migration and M2 polarization of RAW264.7 cells induced by spermine-treated inflammatory MPC-83 cells were reversed by DNMT3B overexpression in inflammatory MPC-83 cells. Finally, *in vivo* experiments revealed that spermine aggravated CP progression and increased M2 macrophage infiltration into the pancreatic tissues of CP mice. **Conclusion**: Our results suggest that increased spermine levels in inflammatory MPC-83 cells aggravated CP progression by promoting macrophage migration and M2 polarization of macrophages, possibly through reduced DNA methylation of *SOX9* and *KRT19*. These findings suggest a novel mechanism underlying the progression of preneoplastic lesions in CP.

Keywords: chronic pancreatitis; spermine; DNA methylation; M2 polarization; macrophages; pancreatic cancer

1. Introduction

Pancreatic cancer (PC) is one of the most lethal cancer types [1]. PC patients usually exhibit no obvious symptoms in the early stage due to an insidious onset, and most cases are diagnosed at an advanced stage, giving rise to a low resectability rate of just 15%. Despite intensive research, the 5-year survival rate of PC after surgery is still only 8% [2]. Chronic pancreatitis (CP) refers to an inflammatory process in which the parenchyma of the pancreas is gradually replaced by fibrotic tissue after irreversible damage to the exocrine and endocrine glands of the pancreas. This eventually results in various changes in the pancreatic tissues and triggers a series of clinical symptoms related to pancreatic inflammation [3]. CP is an independent risk factor for PC [4,5], and clinical studies have shown that the risk of PC in CP patients is much higher than in people without pancreatic fibrosis [6,7]. Therefore, the study of the pathological evolution of CP will help to reveal the mechanisms underlying the transformation of CP into PC. This may provide novel strategies to reverse CP, thereby leading to the prevention and early intervention of PC.

Polyamines such as spermidine, spermine, and putrescine are essential for cell proliferation and differentiation. Maintaining the homeostasis of polyamine metabolism is of great significance for cell survival [8]. Intracellular polyamine metabolism involves biosynthesis, catabolism, and transport. Polyamine catabolism is an irreversible process catalyzed mainly by spermidine/spermine N1-acetyltransferase 1 (SAT1), polyamine oxidase (PAOX), spermine oxidase (SMOX), and diamine

oxidase (DAOX) [9,10]. Dysregulation of polyamine metabolism is associated with various diseases such as cancer [11], cardiovascular diseases [12], and neurodegenerative disorders [13]. Saliva samples from PC patients show significant differences in spermine and N1-acetylspermidine levels compared to a control group. In addition, the saliva samples of CP patients show a significant difference in spermine content compared to controls [14]. Another study reported that polyamines regulate the chromatin accessibility of pancreatic cancer cells (AsPC-1) [15]. Moreover, the gene expression affected by polyamines is related to cell proliferation and differentiation, growth factor and cytokine responses, and starvation responses. Abnormal polyamine metabolism was also shown to affect the activity of enzymes involved in gene methylation, such as DNMT3A/B [16]. Polyamines have been shown to regulate the transcription, translation, and chromatin structure of immune cells, thereby epigenetically regulating immune cells [17,18]. However, the role of polyamine metabolism in CP remains unclear.

In the present study, the pancreatic acinar MPC-83 cell inflammatory model was employed to mimic *in vitro* CP. RNA sequencing was then employed to explore the role of polyamine metabolism in inflammatory MPC-83 cells. Finally, both *in vitro* and *in vivo* experiments were performed to determine whether polyamine metabolism affects CP.

2. Materials and Methods

2.1 Cell Culture and Treatment

MPC-83 cells (YS204C; Yaji Biotechnology Co., Ltd., Shanghai, China) were cultured in RPMI-1640 medium (L210KJ, BasalMedia Technologies Co., Ltd. Shanghai, China) containing 10% fetal bovine serum (FBS, S711-001, LONSERA, Shanghai) and 1% penicillin-streptomycin mixture (G4003, Servicebio Biotechnology Co., Ltd, Wuhan, China) at 37°C with 5% CO_2. IL-6 (10 ng/mL, 90243ES10, Yeasen Biotechnology, Shanghai, China) and TNF-α (20 ng/mL, 90621ES08, Yeasen Biotechnology) were added for 72 h to induce the inflammatory MPC-83 cells, with phosphate buffered saline (PBS, 60158ES, Yeasen Biotechnology) used as the control. Inflammatory MPC-83 cells were further treated with DFMO (100 μM, HY-B0744A, MCE, NJ, USA) or spermine (10 μM, HY-B1777, MCE) for 48 h as described previously [19,20,21]. DMSO (HY-Y0320C, MCE) was used as the control. All cell lines were validated by short tandem repeat (STR) profiling and tested negative for mycoplasma.

2.2 RNA Sequencing

Total RNA was extracted from inflammatory MPC-83 cells, and RNA quality was detected. RNA library construction and transcriptome sequencing (RNA-seq) were completed by a professional sequencing company (TGENE, Shanghai) following standard commercial procedures. Differential expression analysis was performed using edgeR, which calculated differential expression based on read count data aligned to genes, using a negative binomial distribution model. The default criteria for identifying significantly differentially expressed genes (DEGs) were FDR < 0.05 and $|\log2FC| \geq 1$. A gene meeting both criteria was considered a DEG. GO/KEGG pathway enrichment analysis was performed using clusterProfiler with Fisher's exact test for calculation. The Benjamini-Hochberg (BH) method was used for multipletesting correction to control the false discovery rate (FDR), with a corrected p-value threshold of 0.05. GO terms/KEGG pathways meeting this criterion were considered significantly enriched in DEGs.

2.3 Cell Transfection and Treatment

MPC-83 cells were transfected with the overexpression (oe)-DNMT3B or oe-NC via Lipofectamine 2000 (11668027, Invitrogen, Carlsbad, CA, USA). 24h later, the transfected cells were treated with spermine (10 μM, HY-B1777, MCE) for 48 h.

2.4 Cell Viability

Briefly, MPC-83 cells were incubated with 10 μL cell counting kit-8 (CCK-8) reagent for 3 h in the dark at 37 °C. The optical density at 450 nm was measured to assess cell viability via a iMark microplate reader (Bio-Rad, Hercules, CA, USA).

2.5 Flow Cytometry

Briefly, RAW264.7 cells were incubated in the fixative solution (P1110, Solarbio, Beijing, China) for 30 minutes, followed by washing with PBS. Subsequently, the cells were treated with 1% Triton X-100 (T8200, Solarbio) for 10 minutes and washed again with PBS. For flow cytometric gating strategy, forward scatter (FSC-A) and side scatter (SSC-A) dot plots were used to distinguish intact cells from cell debris and aggregates, and single cells were further gated via FSC-A versus FSC-H to eliminate cell doublets and clusters. The resulting single-cell population was added and incubated with APC-labeled anti-mouse CD86 antibody (558703, BD, NJ, USA), FITC-labeled anti-mouse CD86 antibody (553691, BD), or PE-labeled anti-mouse CD206 antibody (568273, BD) at room temperature for 30 minutes. Finally, the cells were analyzed using a BD FACSCalibur flow cytometer (BD Biosciences).

2.6 Quantitative Real-Time Polymerase Chain Reaction (qRT-PCR)

Total RNA extraction from MPC-83 cells was conducted with the R1200 RNA extraction kit (Yuduo, Shanghai, China). The extracted RNA was then reverse-transcribed into complementary DNA (cDNA) using the PC1703 reverse transcription kit (Aidlab Biotechnology Co., Ltd., Beijing, China). Quantitative real-time PCR (qRT-PCR) was performed on a LightCycler 480 Real Time PCR System (Roche, Basel, Switzerland). The relative ex-

pression levels were calculated via the $2^{-\Delta\Delta Ct}$ method, with β-actin serving as the internal reference gene for normalization. The specific primer sequences are detailed below:

β-actin (mouse)-F: 5′-GGCTGTATTCCCCTCCATCG-3′

β-actin (mouse)-R: 5′-CCAGTTGGTAACAATGCCATGT-3′

SAT1 (mouse)-F: 5′-GAGAACACCCCTTCTACCACT-3′

SAT1 (mouse)-R: 5′-GCCTCTGTAATCACTCATCACGA-3′

SMS (mouse)-F: 5′-CACAGCACGCTCGACTTCAA-3′

SMS (mouse)-R: 5′-TGCCATTCTTGTTCGTGTAAGTT-3′

ODC (mouse)-F: 5′-GACGAGTTTGACTGCCACATC-3′

ODC (mouse)-R: 5′-CGCAACATAGAACGCATCCTT-3′

SRM (mouse)-F: 5′-ACATCCTCGTCTTCCGCAGTA-3′

SRM (mouse)-R: 5′- GGCAGGTTGGCGATCATCT-3′

CPA1 (mouse)-F: 5′-CAGTCTTCGGCAATGAGAACT-3′

CPA1 (mouse)-R: 5′-GGGAAGGGCACTCGAACATC-3′

SOX9 (mouse)-F: 5′-GAGCCGGATCTGAAGAGGGA-3′

SOX9 (mouse)-R: 5′-GCTTGACGTGTGGCTTGTTC-3′

KRT19 (mouse)-F: 5′-GGGGGTTCAGTACGCATTGG-3′

KRT19 (mouse)-R: 5′-GAGGACGAGGTCACGAAGC-3′

2.7 Western Blot

Proteins from MPC-83 cell extracts were separated by electrophoresis, transferred onto a nitrocellulose membrane, and then incubated with the following primary antibodies: DNMT3A (1:10,000, 20954-1-AP, Proteintech, Chicago, IL, USA), DNMT3B (1:3000, 26971-1-AP, Proteintech), TET2 (1:1000, 21207-1-AP, Proteintech), NF-κB p65 (1:500, 10745-1-AP, Proteintech), and p-NF-κB (1:5000, 82335-1-RR, Proteintech). β-actin (1:1000, GB11001, Servicebio, Wuhan, China) was used as the internal control. HRP-conjugated IgG served as the secondary antibody. The protein bands were visualized with an enhanced chemiluminescence kit (Vazyme), and the optical density was analyzed using Image-Pro Plus 6.0 software (Media Cybernetics; MD, USA).

2.8 Methylation-Specific PCR (MSP-PCR)

DNA was extracted from MPC-83 cells, and MSP-PCR was performed using the EZ DNA Methylation-Gold Kit as recommended by the manufacturer (Zymo Research, USA). PCR amplification conditions were as follows: 95 ℃ for 1 min, (95 ℃ for 45 secs, 56 ℃ for 30 secs, 72 ℃ for 60 secs) for 35 cycles, 72 ℃ for 10 min. The primers used were as follows:

KRT19-M (mouse)-F: 5′- ATTTTTTTTATTTACGT-GTTTTGGC -3′

KRT19-M (mouse)-R: 5′- CCACGCTTTAATTTC-TAACGAA -3′

KRT19-U (mouse)-F: 5′-GTTATTTTTTTATTTATGTGTTTTGGTG-3′

KRT19-U (mouse)-R: 5′-ATCCCACACTTTAATTTCTAACAAA-3′

JAK3-M (mouse)-F: 5′-GAATTTAGGATTTTCGGAAGAGTC-3′

JAK3-M (mouse)-R: 5′-CCCAAATACTAAAATTAAAAACGTA-3′

JAK3-U (mouse)-F: 5′-TGAATTTAGGATTTTTGGAAGAGTT-3′

JAK3-U (mouse)-R: 5′-CCCAAATACTAAAATTAAAAACATA-3′

SOX9-M (mouse)-F:5′-TTAAGGTCGGCGTGGTTTAC-3′

SOX9-M (mouse)-R:5′-ACTAAAACTTCTACTACGCTCCCG-3′

SOX9-U (mouse)-F:5′-TAGTTTAAGGTTGGTGTGGTTTATG-3′

SOX9-U (mouse)-R:5′-CTAAAACTTCTACTACACTCCCACA-3′

2.9 Enzyme-Linked Immunosorbent Assay (ELISA)

Spermine, spermidine, interleukin-10 (IL-10), and IFN-γ levels were evaluated using the following respective ELISA kits: spermine (EKF59995, Biomatik, Canada), spermidine (EKU11439, Biomatik), IL-10 (E-EL-M0046, Elabscience, Wuhan, China), and IFN-γ (E-EL-M0048, Elabscience).

2.10 Separation of Nucleus and Cytoplasm in MPC-83 Cells

Pre-chilled hypotonic buffer was used to resuspend MPC-83 cells, which were then gently homogenized 40 times on ice. After homogenization, the sample was centrifuged at 1000 ×g for 5 min at 4 ℃, and the supernatant was harvested as the cytoplasmic protein fraction. The residual cell pellet was resuspended in fresh hypotonic buffer and centrifuged under identical conditions. This washing cycle was repeated twice to remove contaminating cytoplasmic components. Subsequently, the purified pellet was lysed with extraction buffer and processed by ultrasonication. The mixture was then centrifuged at 12,000 ×g for 10 min at 4 ℃, and the resultant supernatant was collected as the nuclear protein extract. In the final step, isolated cytoplasmic and nuclear fractions were prepared for Western blot assessment of the NF-κB and phosphorylated NF-κB (p-NF-κB) proteins.

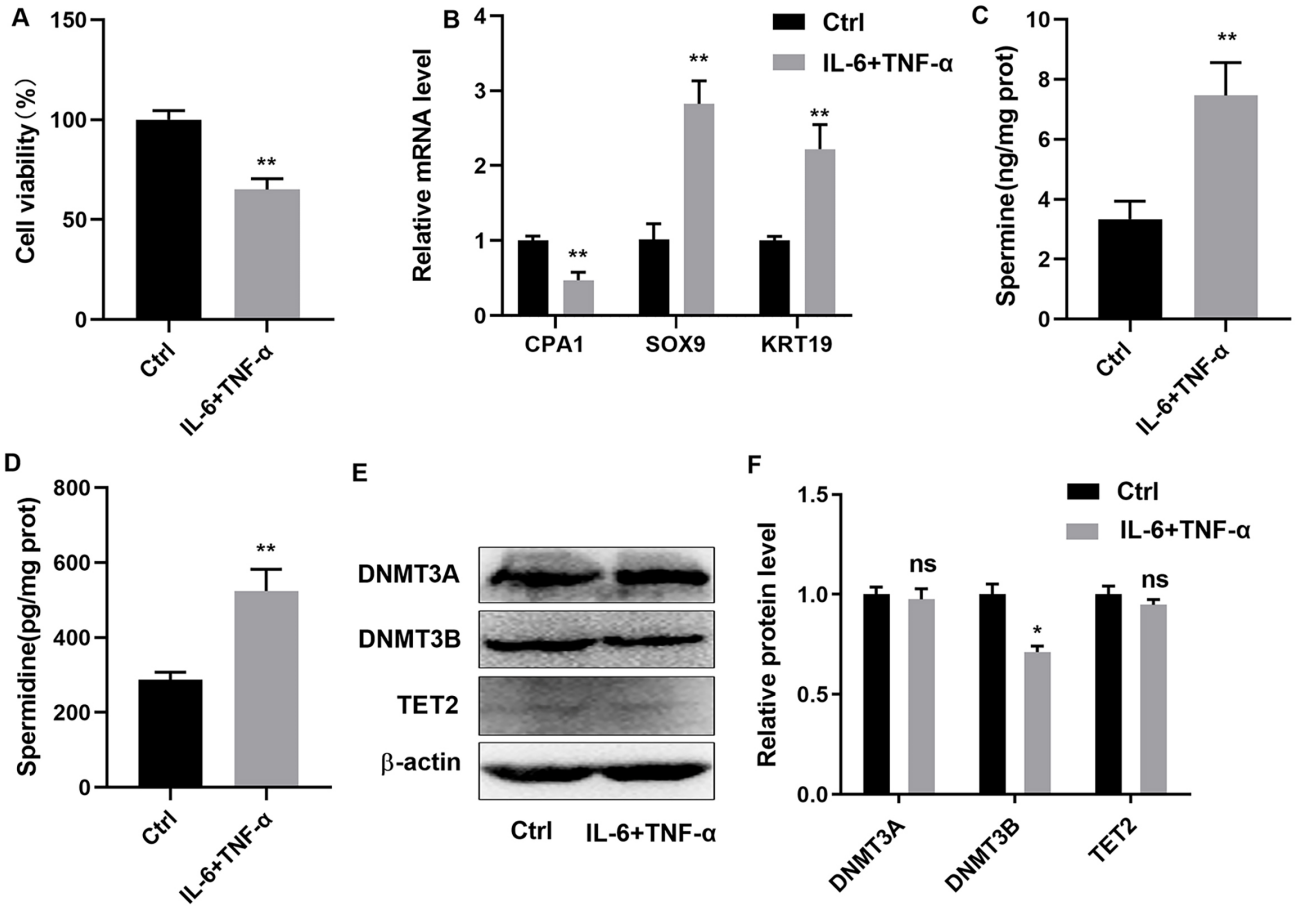

Fig. 1. Successful establishment of the MPC-83 inflammatory model. An inflammatory cell model was established in MPC-83 cells via combined stimulation with IL-6 and TNF-α. (A) CCK-8 assay was used to measure cell viability. (B) qRT-PCR was used to quantify the transcriptional levels of *CPA1*, *SOX9*, and *KRT19*. (C,D) ELISA was used to determine the intracellular spermine and spermidine levels. (E,F) Western blot was used to assess the protein levels of DNMT3A, DNMT3B, and TET2. $*p < 0.05$, $**p < 0.01$, ns indicated no significance. MPC-83, mouse pancreatic acinar carcinoma cell line 83; IL, interleukin; TNF-α, tumor necrosis factor-alpha; CCK-8, cell counting kit-8; qRT-PCR, quantitative real-time polymerase chain reaction; CPA1, carboxypeptidase A1; SOX9, SRY-box 9; KRT19, Keratin 19; ELISA, enzyme-linked immunosorbent assay.

2.11 Transwell Assay

RAW264.7 cell suspension (200 µL) was seeded into upper Transwell inserts, and 600 µL of complete medium supplemented with serum was added to the lower compartment. The whole culture system was incubated at 37 °C with 5% CO_2 for 48 h. After incubation, the residual medium in the upper inserts was carefully removed, and the inner surface of each insert was gently wiped. Samples were rinsed twice using pre-warmed PBS solution. Thereafter, the cells were fixed in 4% paraformaldehyde for 30 min at room temperature, followed by staining with 0.1% crystal violet for 10 min. Finally, migrated cells were observed and photographed under an inverted microscope (OLYMPUS IX73, Tokyo, Japan).

2.12 Co-Culture of MPC-83 and RAW264.7 Cells

RAW264.7 cells (GDC0143, CCTCC) were cultured in high-glucose DMEM (G4511; Servicebio) supplemented with 10% FBS (S711-001, LONSERA) and 1% penicillin-streptomycin solution (G4003, Servicebio) at 37 °C with 5% CO_2, and cells were collected at passages 10–25. MPC-83 cells at passages 15–20 were seeded in the upper Transwell inserts, while RAW264.7 cellswere plated in the lower chamber. The two cell types were co-cultured for 24 h at a ratio of 1:2 (MPC-83 to RAW264.7). Cell culture supernatants and cellular samples were harvested for subsequent assessment.

2.13 Establishment of the CP Mouse Model and Experimental Group

SPF-grade male C57 mice weighing 21–27 g (Cavens, Changzhou, China), aged 8–10 weeks, were employed in this study. Before experiments, mice were acclimated for 1 week. All mice were provided free and unlimited access to normal chow and water, housed under suitable temperature (22 ± 2 °C) and humidity (65% ± 5%) with a 12/12-h

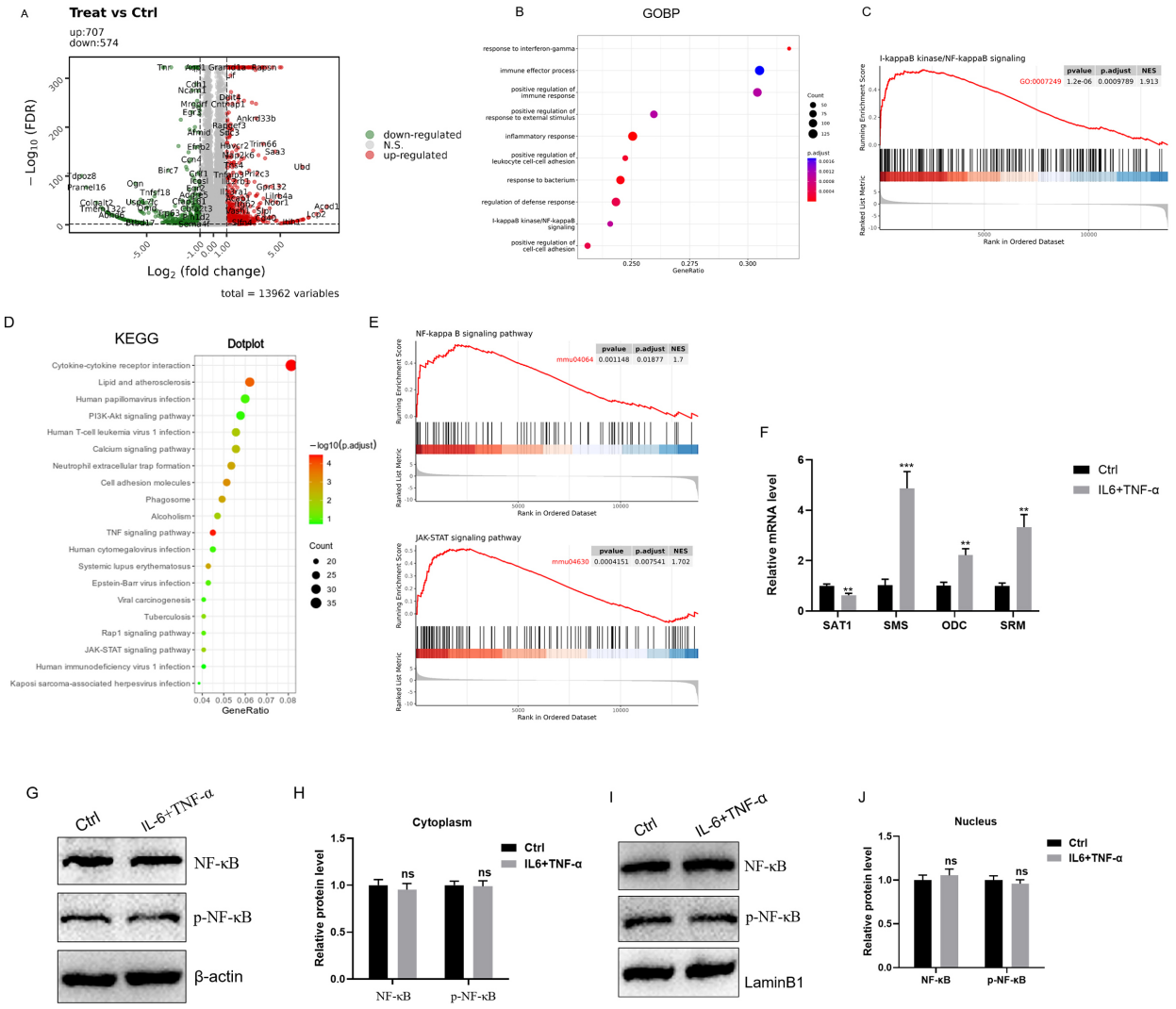

Fig. 2. Inflammatory MPC-83 cells exhibit abnormal polyamine metabolism. MPC-83 cells were first subjected to IL-6/TNF-α stimulation. RNA-sequencing was subsequently performed to identify differentially expressed genes, with the results visualized as a volcano plot (A). Based on the RNA-sequencing data, GOBP analysis (B) and GSEA plots (C) were conducted to assess enrichment of the IKB/NF-κB signaling pathway. KEGG pathway analysis (D) and GSEA plots (E) were performed to verify enrichment of the NF-κB and JAK/STAT signaling pathways. (F) qRT-PCR was used to determine the mRNA expression levels of *ODC*, *SMS*, *SRM*, and *SAT1*. (G–J) Western blot analysis was used to determine the protein levels of NF-κB and p-NF-κB in both the cytoplasmic and nuclear fractions of MPC-83 cells. $^{**}p < 0.01$, $^{***}p < 0.001$, ns indicated no significance. GOBP, Gene Ontology Biological Process; GSEA, Gene Set Enrichment Analysis; KEGG, Kyoto Encyclopedia of Genes and Genomes; ODC, ornithine decarboxylase; SMS, spermidine to spermine; SRM, spermidine synthase; SAT1, spermidine/spermine N1-acetyltransferase 1.

light/dark cycle. Only healthy mice without congenital defects and with qualified body weight were included. Animals that died accidentally, suffered severe injury or unrelated complications during the experiment were excluded. A double-blind design was applied. Mice were randomly divided into four groups (n = 6) [22,23], Sham, Model, Model + DFMO, and Model + Spermine. For the construction of the CP model, mice were injected intraperitoneally with ceruletide (50 μg/kg, HY-A0190, MCE) three times a week for 6 weeks. The sham group was injected intraperitoneally with the same amount of PBS. Following the establishment of the CP model, mice in the Model + DFMO and Model + Spermine groups were injected intraperitoneally with DFMO (20 mg/kg, HY-B0744A, MCE) and Spermine (20 mg/kg, HY-B1777, MCE) once a day for three days. Finally, all mice were anesthetized with isoflurane (3.0% isoflurane to induce anesthesia, followed by 1.5% isoflurane to maintain anesthesia). After the collection of blood

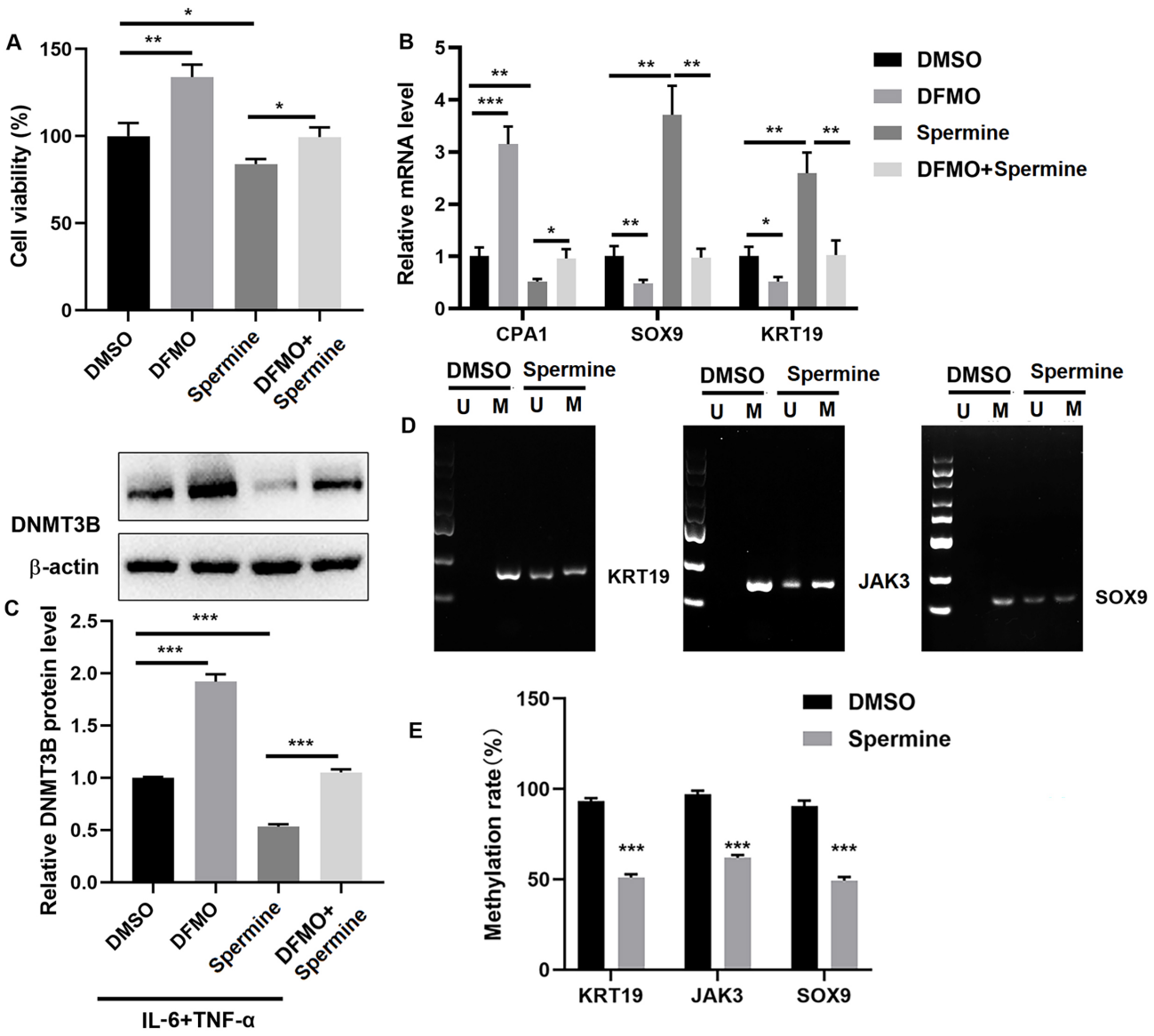

Fig. 3. Polyamine metabolism affects inflammatory MPC-83 cells by reducing DNA methylation. MPC-83 cells were first stimulated with IL-6 and TNF-α, followed by treatment with DFMO or spermine (DMSO was the control). (A) CCK-8 assay was used to evaluate cell viability. (B) qRT-PCR was employed to quantify the mRNA levels of *CPA1*, *SOX9*, and *KRT19*. (C) Western blot was used to determine the protein levels of DNMT3B. (D,E) MSP-PCR was used to determine DNA methylation of *JAK3*, *SOX9*, and *KRT19* in MPC-83 cells. *$p < 0.05$, **$p < 0.01$, ***$p < 0.001$. U, unmethylated; M, methylated.

samples from the tail vein, the mice were sacrificed by cervical dislocation, and the pancreatic tissues were collected.

2.14 Hematoxylin-Eosin (HE) and Masson Staining

Following fixation in 4% formaldehyde solution, pancreatic specimens were paraffin-embedded and cut into continuous sections of 5 μm thickness. HE staining was performed with a commercial kit (G1120, Solarbio, Beijing) to observe histopathological alterations in the pancreatic tissues. Masson's trichrome staining (G1340, Solarbio, Beijing) was used to assess the degree of pancreatic fibrosis. All histological images were acquired with an OLYMPUS BX63 light microscope (Tokyo, Japan).

2.15 Immunohistochemical (IHC) Staining

After 24 h of fixation in 4% paraformaldehyde at 4 °C, pancreatic tissues underwent dehydration and clearing, followed by paraffin embedding and sectioning at a thickness of 5 μm. Tissue sections were first treated with 3% hydrogen peroxide (Thermo Scientific, Carlsbad, CA, USA) for 8 min at ambient temperature, then blocked with 10% goat serum (16210064, Gibco, Carlsbad, CA, USA) for 30 min under the same conditions. Subsequently, the sections were incubated overnight at 4 °C with the following primary antibodies: anti-CD86 (1:100, 19589S, CST), anti-CD206 (1:200, 24595S, CST), and anti-α-SMA (1:3000, 14395-1-

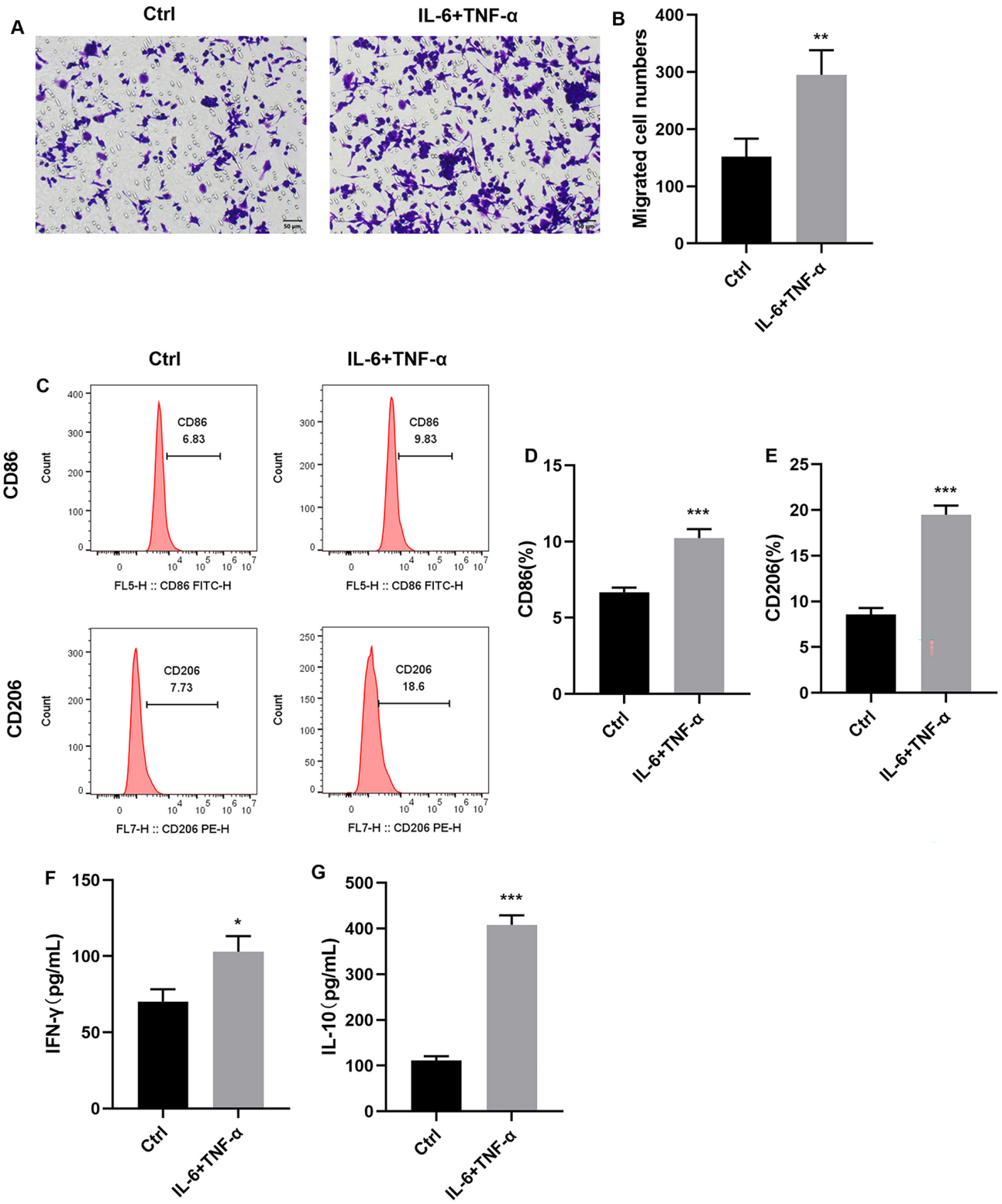

Fig. 4. IL-6/TNF-α-treated MPC-83 cells promote migration and alter M1/M2 polarization of RAW264.7 cells. RAW264.7 macrophages were co-cultured with MPC-83 cells pre-stimulated with IL-6 and TNF-α. (A,B) Transwell assay was used to quantify the migratory potential of RAW264.7 cells. Scale bar: 50 μm. (C–E) Flow cytometric analysis was utilized to assess the percentage of $CD86^+$-RAW264.7 and $CD206^+$-RAW264.7 cells. (F,G) ELISA was employed to measure the levels of IFN-γ and IL-10 in RAW264.7 cells. $*p < 0.05$, $**p < 0.01$, $***p < 0.001$.

AP, Proteintech). After primary incubation, samples were reacted with HRP-conjugated recombinant goat anti-rabbit secondary antibody (H+L) (1:4000, RGAR011, Proteintech) for 30 min at room temperature. DAB chromogenic reaction and hematoxylin counterstaining were conducted sequentially for 10 min at room temperature. Finally, histological images were recorded with an OLYMPUS BX63 light microscope (Tokyo, Japan).

2.16 Statistical Analysis

All *in vitro* assays were conducted with three separate biological replicates. Quantitative data processing was performed using GraphPad Prism 7.0 software (La Jolla, CA, USA), and all results were expressed as the mean ± SD. Intergroup differences were assessed with the unpaired *t*-test or one-way ANOVA, and Tukey's multiple comparison test was applied for subsequent post hoc analysis. A p-value of < 0.05 was defined as the threshold for statistical significance.

3. Results

3.1 The MPC-83 Inflammatory Model was Successfully Established and Exhibited Abnormal Polyamine Metabolism

MPC-83 is a homogeneous and stable cell line derived from the mouse pancreas. These cells exhibit typical acinar cell phenotypes and are highly consistent with the key damaged cells in CP, allowing consistent and reproducible induction of an inflammatory microenvironment *in vitro*. In the present study, MPC-83 cells were used for the *in vitro* experiments, while *in vivo* experiments were performed in mice. An inflammatory cell model was constructed by stimulating MPC-83 cells with IL-6 and TNF-α. This combined cytokine intervention markedly suppressed cell viability (Fig. 1A). Furthermore, the mRNA level of acinar marker carboxypeptidase A1 (CPA1) was downregulated following IL-6/TNF-α stimulation, whereas the ductal metaplasia-related genes SRY-box 9 (*SOX9*) and Keratin 19 (*KRT19*) were markedly upregulated (Fig. 1B), indicating the occurrence of pancreatic acinar-to-ductal metaplasia (ADM). ELISA revealed that intracellular spermine and spermidine levels were increased in cytokine-exposed MPC-83 cells (Fig. 1C,D), whereas the protein level of DNA methyltransferase 3b (DNMT3B) was decreased (Fig. 1E,F). To further explore the molecular changes under inflammatory conditions, transcriptomic profiling via RNA-seq was performed to screen for differentially expressed genes. Volcano plot analysis identified 707 upregulated and 574 downregulated genes in the cytokine-treated group relative to controls (Fig. 2A). Significant differences were observed in genes related to polyamine metabolism, such as the key upstream rate-limiting enzyme for polyamine synthesis (ornithine decarboxylase, *ODC*), the metabolic enzyme for converting spermidine to spermine (*SMS*), and the polyamine catabolic enzyme *SAT1* (Table 1). qRT-PCR analysis further revealed that IL-6/TNF-α treatment significantly increased the mRNA expression of *ODC*, *SMS*, and spermidine synthase (*SRM*), while decreasing *SAT1* mRNA expression (Fig. 2F). Gene Ontology Biological Process (GOBP) analysis and Gene Set Enrichment Analysis (GSEA) revealed the IκB/NF-κB pathway was significantly enriched following IL-6/TNF-α treatment (Fig. 2B,C). Kyoto Encyclopedia of Genes and Genomes (KEGG) analysis and GSEA further identified significant enrichment of the NF-κB and JAK/STAT pathways (Fig. 2D,E). However, Western blot analysis revealed that total and phosphorylated protein levels of NF-κB remained unchanged in both the cytoplasmic (Fig. 2G,H) and nuclear (Fig. 2I,J) fractions after cytokine intervention (Fig. 2G–J). Collectively, these findings demonstrate that inflammatory stress induced by IL-6 and TNF-α can effectively trigger abnormal polyamine metabolism in MPC-83 cells.

3.2 Polyamine Metabolism Affects Inflammatory MPC-83 Cells by Reducing DNA Methylation

Next, we explored the underlying mechanisms by which polyamine metabolism affected inflammatory MPC-83 cells. Functional analysis via CCK-8 showed that DFMO, a specific irreversible ODC inhibitor, reversed the decreased cell viability triggered by IL-6/TNF-α stimulation. In contrast, supplementary spermine partly abolished this protective effect (Fig. 3A). In inflammatory MPC-83 cells, DFMO intervention upregulated the acinar marker *CPA1* and downregulated ADM-related *SOX9* and *KRT19* at the transcriptional level. However, co-treatment with spermine largely counteracted the above changes (Fig. 3B). Western blot results demonstrated that DFMO-mediated upregulation of DNMT3B protein was also markedly reversed following the addition of spermine (Fig. 3C). MSP-PCR analysis further revealed that spermine reduced DNA methylation of *JAK3*, *SOX9*, and *KRT19* in MPC-83 cells (Fig. 3D,E). These results indicate that polyamine metabolism regulates acinar cell function by reducing DNA methylation.

3.3 IL-6/TNF-α-Treated MPC-83 Cells Promote Migration and M1/M2 Polarization of RAW264.7 Cells

We next investigated the regulatory effect of IL-6/TNF-α-stimulated MPC-83 cells on macrophage functions. Transwell migration assay showed that conditioned MPC-83 cells (pretreated with IL-6 and TNF-α) significantly enhanced the migratory capacity of RAW264.7 macrophages (Fig. 4A,B). Flow cytometric analysis revealed a notable increase in the proportion of $CD86^+$-RAW264.7 and $CD206^+$-RAW264.7 cells following co-culture with IL-6/TNF-α-treated MPC-83 cells (Fig. 4C–E). Additionally, the levels of IFN-γ and IL-10 in RAW264.7 cells increased significantly after co-culture with inflamed MPC-83 cells (Fig. 4F,G). Taken together, these findings indicate that IL-6/TNF-α-induced inflamma-

Table 1. Genes related to the polyamine metabolism and NF-κB/JAK-STAT pathways.

Gene symbol	logFC	logCPM	*p*-value	logPval	*p*_adjusted
Odc1	1.019342211	9.72790822	0	Inf	0
Sms	0.389575225	5.865407164	1.36×10^{-89}	88.86653433	8.26×10^{-89}
Sat1	–0.097686666	8.319482687	1.72×10^{-30}	29.76490287	5.20×10^{-30}
Ass1	0.49421575	4.534501148	3.49×10^{-58}	57.45745516	1.54×10^{-57}
Nfkbia	1.322487737	5.968289384	0	Inf	0
Nfkbie	1.143964921	5.399724386	0	Inf	0
Jak3	1.104609879	5.024046562	0	Inf	0
Stat5a	0.140801882	4.170813231	5.11×10^{-5}	4.291301852	7.89×10^{-5}
Stat3	0.97739172	6.74531934	0	Inf	0

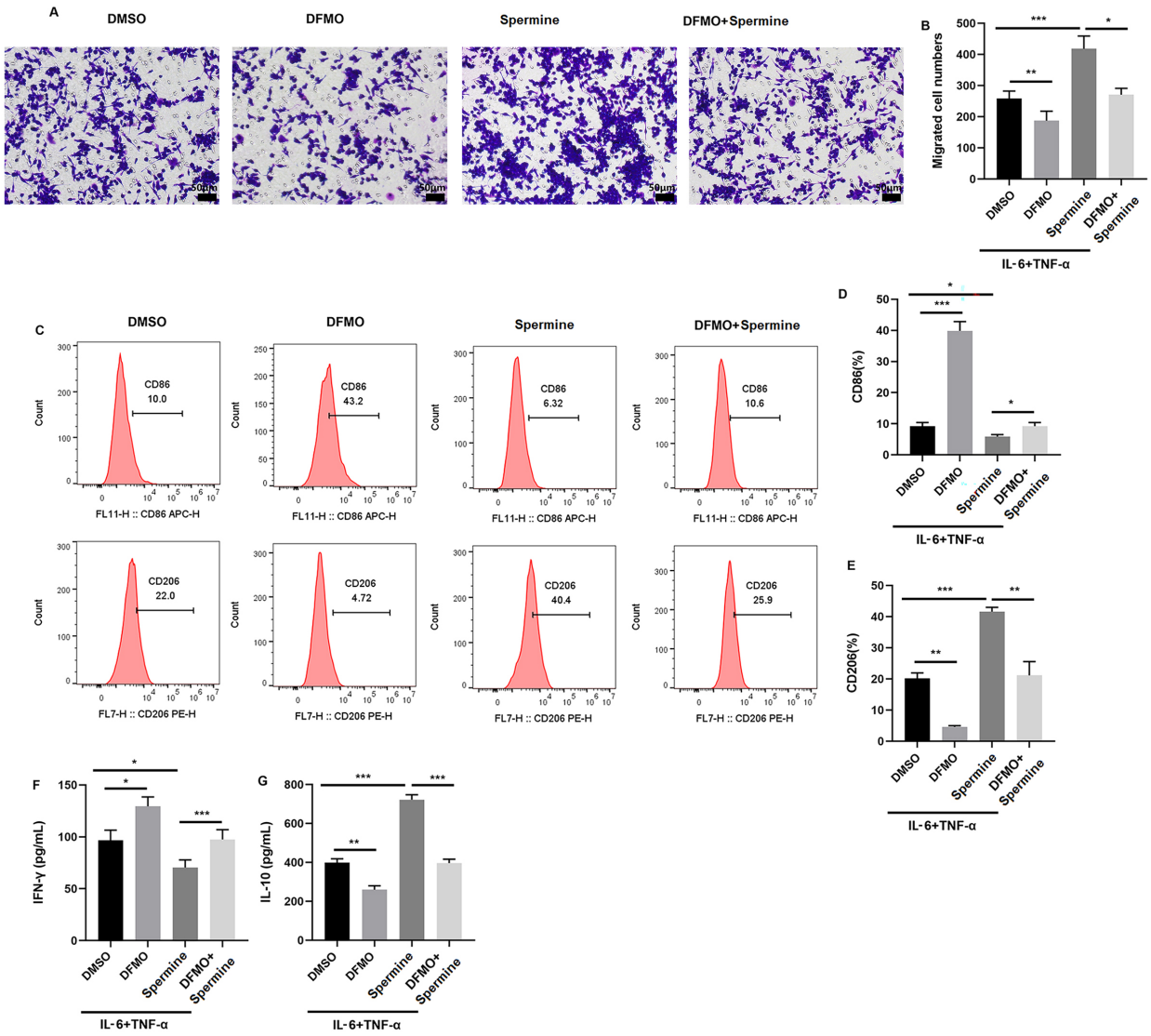

Fig. 5. Spermine treatment of IL-6/TNF-α-treated MPC-83 cells promotes the migration and M2 polarization of RAW264.7 cells. MPC-83 cells pre-stimulated with IL-6 and TNF-α were treated with DFMO, spermine, DFMO + spermine, or DMSO (control group), followed by co-culture with RAW264.7 macrophages. (A,B) The Transwell assay was used to quantify the migratory potential of RAW264.7 cells. Scale bar: 50 μm. (C–E) Flow cytometric analysis was utilized to determine the percentage of $CD86^+$- RAW264.7 and $CD206^+$-RAW264.7 cells. (F,G) ELISA was used to measure the concentrations of IFN-γ and IL-10 in RAW264.7 cells. $*p < 0.05$, $**p < 0.01$, $***p < 0.001$.

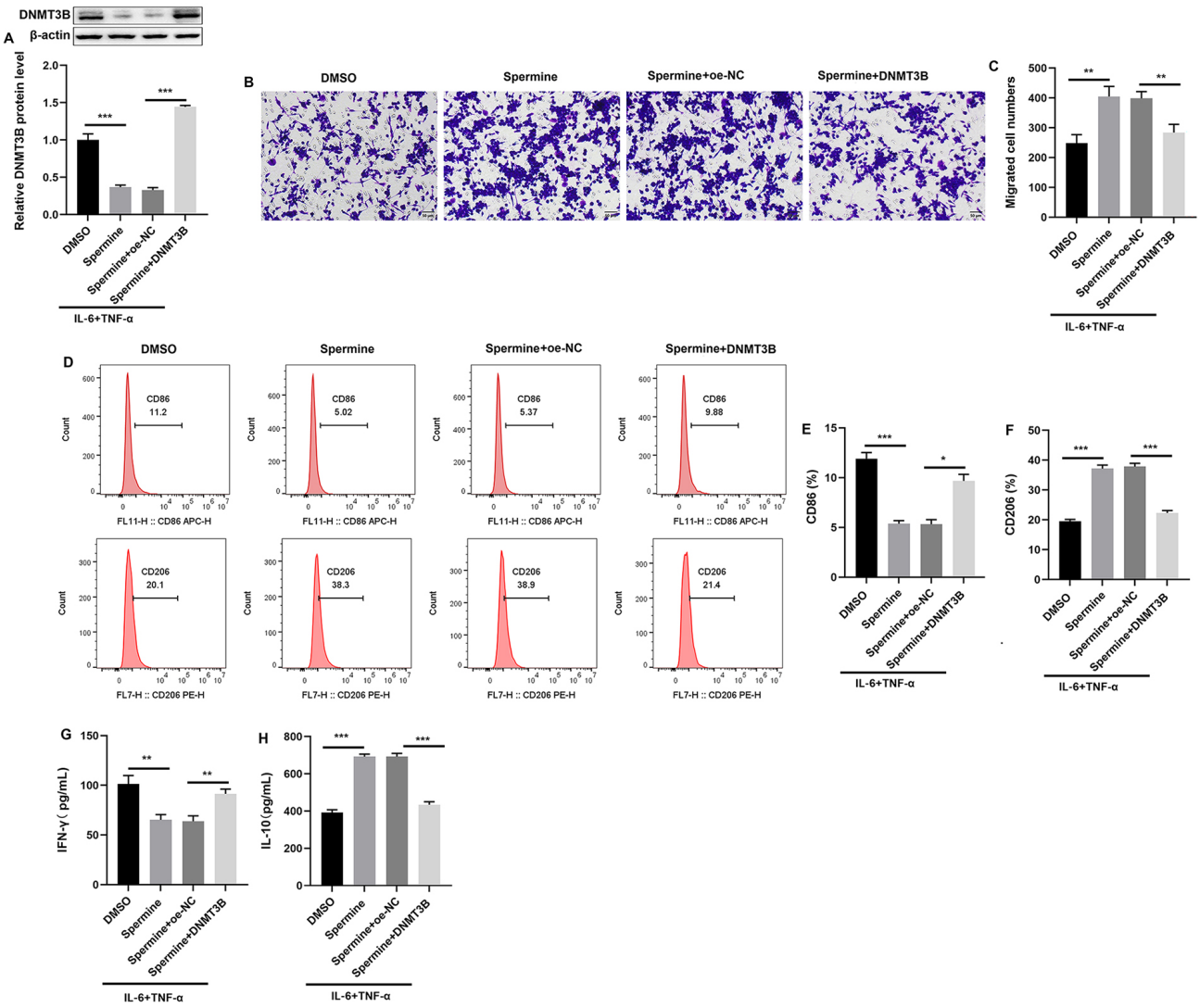

Fig. 6. DNMT3B overexpression in IL-6/TNF-α-treated MPC-83 cells inhibits the migration and M2 polarization of RAW264.7 cells. MPC-83 cells pre-stimulated with IL-6 and TNF-α were transfected with the DNMT3B overexpression vector for 48 h, treated with spermine (DMSO served as the control group), and subsequently co-cultured with RAW264.7 cells. (A) Western blot was used to quantify the protein abundance of DNMT3B in MPC-83 cells. (B,C) Transwell assay was used to evaluate the migratory potential of RAW264.7 cells. Scale bar: 50 µm. (D–F) Flow cytometric analysis was employed to determine the percentage of $CD86^+$-RAW264.7 and $CD206^+$-RAW264.7 cells. (G,H) ELISA was used to assess the concentrations of IFN-γ and IL-10 in RAW264.7 cells. $*p < 0.05$, $**p < 0.01$, $***p < 0.001$.

tory MPC-83 cells can modulate the migration and polarization of macrophages.

3.4 Dysregulated Polyamine Metabolism in IL-6/TNF-α-Treated MPC-83 Cells Affects the Migration and M1/M2 Polarization of RAW264.7 Cells

DFMO-treated inflammatory MPC-83 cells were found to significantly reduce the migration of RAW264.7 cells. This was reversed by spermine-treated inflammatory MPC-83 cells (Fig. 5A,B). Also, spermine-treated inflammatory MPC-83 cells markedly reversed the increase in $CD86^+$-RAW264.7 cells and the decrease in $CD206^+$-RAW264.7 cells induced by DFMO-treated inflammatory MPC-83 cells (Fig. 5C–E). Similarly, DFMO-treated inflammatory MPC-83 cells increased the IFN-γ level (Fig. 5F) and reduced the IL-10 level (Fig. 5G) in RAW264.7 cells. This was significantly reversed by spermine-treated inflammatory MPC-83 cells. The above results suggest that spermine treatment of inflammatory MPC-83 cells promotes the migration and M2 polarization of macrophages.

3.5 DNMT3B Overexpression in IL-6/TNF-α-Treated MPC-83 Cells Affects the Migration and M1/M2 Polarization of RAW264.7 Cells

DNMT3B was overexpressed in IL-6/TNF-α-treated MPC-83 cells (Fig. 6A). Spermine-treated inflammatory

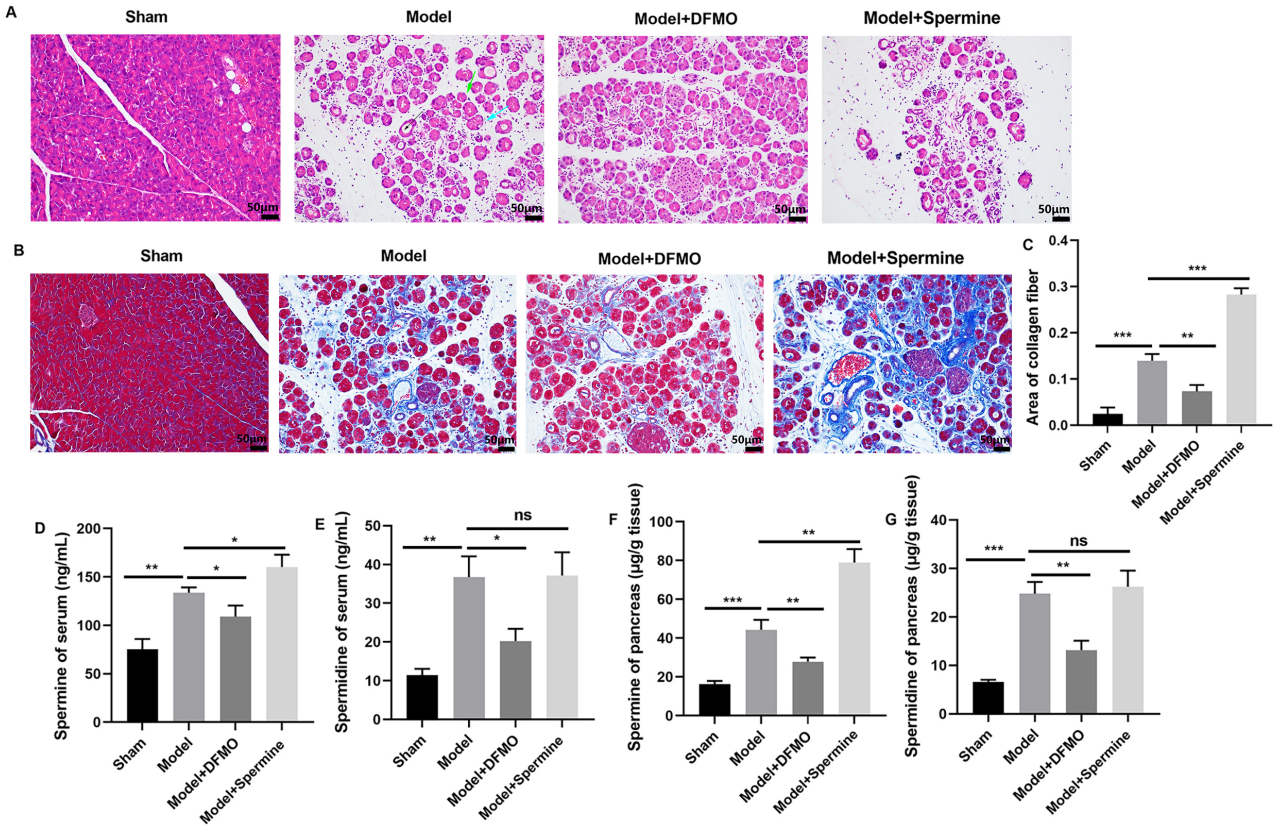

Fig. 7. Spermine aggravates CP progression *in vivo*. CP mice (n = 6) were injected with DFMO or spermine. HE staining (A) and Masson staining (B,C) were employed to assess the pathological changes and collagen fibers in the pancreatic tissues of mice. Scale bar: 50 μm, necrotic acini (black arrow), enlarged acini and stroma (green arrow), infiltrated inflammatory cells (blue arrow). ELISA was employed to evaluate spermine and spermidine levels, both in serum (D,E) and pancreatic tissues (F,G). *$p < 0.05$, **$p < 0.01$, ***$p < 0.001$, ns indicated no significance.

MPC-83 cells were found to significantly increase the migration of RAW264.7 cells. This was reversed by inflammatory MPC-83 cells that overexpressed DNMT3B (Fig. 6B,C). Inflammatory MPC-83 cells that overexpressed DNMT3B reversed the decrease in $CD86^+$-RAW264.7 cells and the increase in $CD206^+$-RAW264.7 cells induced by spermine-treated inflammatory MPC-83 cells (Fig. 6D–F). In addition, the decrease in IFN-γ level (Fig. 6G) and increase in IL-10 level (Fig. 6H) in RAW264.7 cells induced by spermine-treated inflammatory MPC-83 cells were reversed by inflammatory MPC-83 cells overexpressing DNMT3B. These results suggest that DNMT3B overexpression in inflammatory MPC-83 cells inhibits the migration and M2 polarization of macrophages.

3.6 Spermine Aggravates CP Progression and Enhances M2 Macrophage Infiltration in Vivo

For the *in vivo* experiments, CP mice were injected with DFMO or spermine. HE staining revealed disrupted acinar structure in the model group, as manifested by necrotic acini (black arrow), enlarged acini and stroma (green arrow), and a large number of infiltrated inflammatory cells (blue arrow). These features were more pronounced after spermine treatment, but were mitigated by DFMO (Fig. 7A). Masson staining of the model group revealed a large amount of blue collagen fibers in the pancreatic tissues, which were enhanced by spermine, and attenuated by DFMO (Fig. 7B,C). ELISA analysis revealed that DFMO significantly reversed the increased spermine and spermidine levels in model mice, both in the serum (Fig. 7D,E) and pancreatic tissues (Fig. 7F,G). Spermine alone enhanced the increased spermine in both the serum (Fig. 7D) and pancreatic tissues (Fig. 7F) of model mice. Additionally, immunohistochemical analysis revealed that spermine significantly enhanced the increased expression of α-SMA (Fig. 8A,B) and CD206 (Fig. 8E,F) in model mice, while reversing the increased CD86 expression (Fig. 8C,D). DFMO induced the opposite effects (Fig. 8A–F).

4. Discussion

Polyamine homeostasis is tightly maintained in normal cells via feedback modulation of the metabolic network, but this balanced state is frequently disrupted in tumor cells. Tumor growth and disease progression rely on an

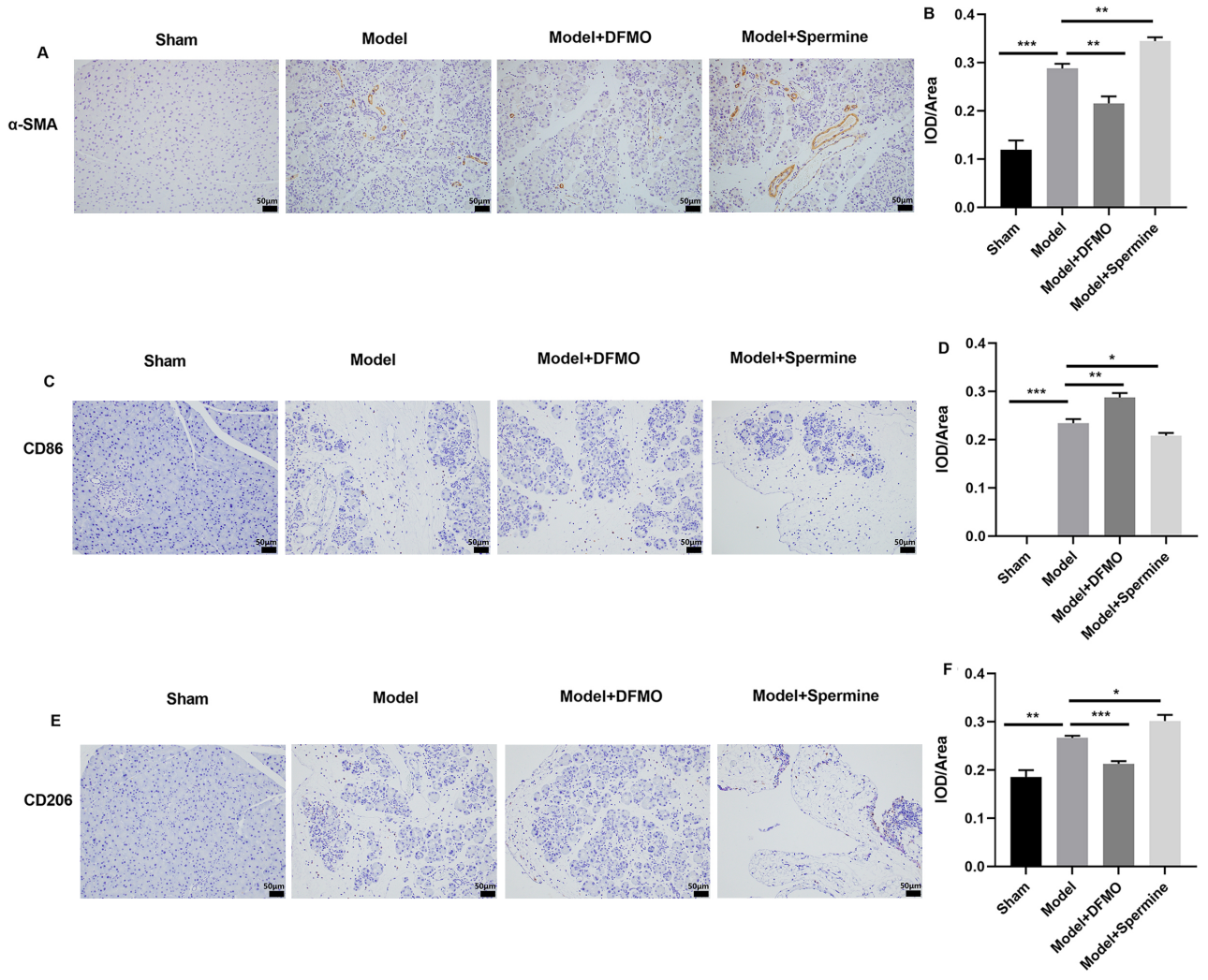

Fig. 8. Spermine enhances M2 macrophage infiltration in the pancreatic tissue of CP mice. CP mice (n = 6) were injected with DFMO or spermine. Immunohistochemical analysis was employed to detect the expression of α-SMA (A,B), CD86 (C,D), and CD206 (E,F) in mice, Scale bar: 50 μm. *$p < 0.05$, **$p < 0.01$, ***$p < 0.001$.

elevated level of intracellular polyamine to facilitate malignant cell proliferation, invasion, and metastasis [24]. Aberrant polyamine metabolism in malignancies is primarily characterized by upregulated synthetic enzymes and accumulated polyamine metabolites [25]. Fölsch and colleagues [26] first reported the involvement of polyamines in pancreatic development in the 1990s. These authors found that pancreatic cell proliferation correlated with the early rise in ODC activity, which drives putrescine generation. Uimari et al. [27] reported that SAT1 overexpression alleviates the pathological severity of zinc-triggered pancreatitis in mice. Similarly, Räsänen et al. [28] found that enhanced pancreatic polyamine catabolism contributes to acute pancreatitis in SAT1-overexpressing transgenic rats. Moreover, Lee et al. [15] reported that knockout of oncogenic Kras in pancreatic cancer cells downregulates the transcriptional levels of polyamine synthetic genes, including *ODC1*, *SRM*, and *SMS*. Collectively, these studies indicate that polyamine metabolic reprogramming acts as a critical molecular bridge linking pancreatitis to pancreatic cancer.

In the present study, combined IL-6 and TNF-α treatment was used to stimulate MPC-83 cells to mimic CP *in vitro*. Spermine and spermidine levels were found to be significantly elevated in IL-6/TNF-α-treated MPC-83 cells. Furthermore, RNA-sequencing revealed dysregulated polyamine metabolism in these cells, while qRT-PCR showed increased *ODC*, *SMS* and *SRM* expressions, and decreased *SAT1* expression. In addition, GOBP, KEGG, and GSEA analyses drew our attention to the NF-κB pathway. NF-κB is a nuclear transcription factor with multidirectional regulatory functions. It is activated by factors such as inflammatory stimuli and regulates the expression of various cell chemokines and adhesion molecules at the transcriptional level, thereby participating in the progres-

sion of acute pancreatitis [29,30]. The upregulation of inflammatory mediators further promotes the nuclear translocation and activation of NF-κB, forming a positive feedback loop. This amplifies the inflammatory effect and aggravates acute pancreatitis, thereby affecting the prognosis of patients [31]. However, Western blot analysis revealed that IL-6 and TNF-α treatment of MPC-83 cells had no significant effect on NF-κB and p-NF-κB protein levels in the cytoplasm and nucleus, which was inconsistent with the results of RNA sequencing analysis. It was possible that transcriptome profiling reflected instantaneous mRNA transcription, whereas protein expression was further modulated by post-transcriptional regulation, translational repression, mRNA stability, and ubiquitin-mediated protein degradation. In addition, pathway enrichment was a statistical result based on the overall gene set rather than relying solely on core marker proteins. Perhaps the additional studies with more samples were needed to further clarify the role of NF-κB in CP.

Pancreatitis associated with tissue damage acts in conjunction with the activated Kras oncogene, releasing the epigenetic reprogramming required for tumor transformation, and ultimately leading to PC [32,33]. DNA methylation was one of the first reported epigenetic changes and is mediated by DNMTs, such as DNMT1, DNMT3A, and DNMT3B [34]. It is generally believed that chronic inflammation promotes DNA methylation [35]. However, in the current study, IL-6 and TNF-α treatment reduced the protein level of DNMT3B. This was further reduced by spermine, but reversed by DFMO. Furthermore, MSP-PCR analysis revealed that spermine reduced DNA methylation of *JAK3*, *SOX9*, and *KRT19* in MPC-83 cells, suggesting that polyamine metabolism regulates acinar cell functions by reducing DNA methylation. Elucidation of this specific mechanism requires further study.

Polyamines can also exert immunosuppressive effects. They facilitate intrinsic immune evasion through favorable epigenetic modifications or DNA stabilization, thereby helping tumor cells resist attack by cytotoxic lymphocytes [36]. Travers et al. [37] reported that combined use of DFMO and the epigenetic agent 5-azacytidine significantly reduced M2-polarized macrophages, increased M1-polarized tumor-killing macrophages, and extended the survival of tumor-bearing mice. Tumor-associated macrophages play a pivotal role in constructing an immunosuppressive tumor microenvironment, thereby enabling cancer cells to escape immune surveillance [38]. The expression levels of ODC1 and SMS in ovarian cancer are closely associated with a decrease in immune cell infiltration [39]. Consistent with these findings, the present study found that spermine exacerbated the progression of CP and promoted M2 macrophage infiltration in the pancreatic tissues of CP mice. This is also consistent with the results reported by Yang et al. [40]. Furthermore, the current *in vitro* experiments showed that IL-6/TNF-α-treated MPC-83 cells promoted the migration and M2 polarization of RAW264.7 cells, with this effect further enhanced by spermine treatment. Notably, the promotion of RAW264.7 cell migration and M2 polarization induced by spermine-treated inflammatory MPC-83 cells could be reversed by overexpressing DNMT3B in inflammatory MPC-83 cells.

5. Limitations

1. MPC-83 cells are mouse pancreatic acinar cells. The lack of validation in primary cells or organoid models limits the extrapolation of conclusions reached by IL-6/TNF-α stimulation of MPC-83 cells.

2. IL-6 and TNF-α were employed to induce chronic inflammation in MPC-83 cells and thus mimic the CP model *in vitro*. However, this may not fully recapitulate the authentic pathological characteristics of CP driven by multicellular interactions and multi-factor synergistic effects in the complex microenvironment of CP.

3. The specific molecular interaction mechanisms by which spermine regulates DNMT3B (e.g., direct binding, ubiquitin-mediated degradation, or transcriptional regulation) remain unclarified and require further investigation in future studies.

6. Conclusions

In summary, our results showed that increased spermine levels in inflammatory MPC-83 cells promote the migration and M2 polarization of macrophages, thereby promoting CP progression. This may involve reduced DNA methylation in MPC-83 cells. Our study suggests a novel mechanism underlying the progression of preneoplastic lesions in CP.

Availability of Data and Materials

The datasets used and analyzed during the current study are available from the corresponding authors upon reasonable request.

Author Contributions

YZ contributed to conception and design, acquisition of data, analysis and interpretation of data; HW contributed to the acquisition of data, analysis and interpretation of data. XS contributed to the acquisition of data. YLing participated in the analysis and interpretation of data, drafted the manuscript and reviewed it critically for important intellectual content. YLiu participated in the conception and design of the work and agreed to be accountable for all aspects of the work in ensuring that questions related to the accuracy or integrity of any part of the work are appropriately investigated and resolved. All authors read and approved the final manuscript to be published. All authors contributed to editorial changes in the manuscript. All authors have participated sufficiently in the work and agreed to be accountable for all aspects of the work.

Ethics Approval and Consent to Participate

This study was approved by the Laboratory Animal Center Welfare and Ethics Committee of Nantong University (No. P20250311-003). The study was carried out in accordance with the ARRIVE guidelines. All animal experiments complied with the NIH Guide for the Care and Use of Laboratory Animals (8th edition) and national regulations on laboratory animal management.

Acknowledgment

The Graphical Abstract was created by us using Photoshop (Adobe Systems Inc., San Jose, CA, USA).

Funding

This study was supported by Wuxi City Traditional Chinese Medicine Science and Technology Development Plan Project (No. ZYYB202420).

Conflicts of Interest

The authors declare no conflicts of interest.

Supplementary Material

Supplementary material associated with this article can be found, in the online version, at https://doi.org/10.31083/FBL51641.

References

[1] Bray F, Laversanne M, Sung H, Ferlay J, Siegel RL, Soerjomataram I, et al. Global cancer statistics 2022: GLOBOCAN estimates of incidence and mortality worldwide for 36 cancers in 185 countries. CA: a Cancer Journal for Clinicians. 2024; 74: 229–263. https://doi.org/10.3322/caac.21834

[2] Sung H, Ferlay J, Siegel RL, Laversanne M, Soerjomataram I, Jemal A, et al. Global Cancer Statistics 2020: GLOBOCAN Estimates of Incidence and Mortality Worldwide for 36 Cancers in 185 Countries. . CA: a Cancer Journal for Clinicians. 2021; 71: 209–249. https://doi.org/10.3322/caac.21660

[3] Singh VK, Yadav D, Garg PK. Diagnosis and Management of Chronic Pancreatitis: A Review. JAMA. 2019; 322: 2422–2434. https://doi.org/10.1001/jama.2019.19411

[4] Multhoff G, Molls M, Radons J. Chronic inflammation in cancer development. Frontiers in Immunology. 2012; 2: 98. https://doi.org/10.3389/fimmu.2011.00098

[5] Kirkegård J, Cronin-Fenton D, Heide-Jørgensen U, Mortensen FV. Acute Pancreatitis and Pancreatic Cancer Risk: A Nationwide Matched-Cohort Study in Denmark. Gastroenterology. 2018; 154: 1729–1736. https://doi.org/10.1053/j.gastro.2018.02.011

[6] Kirkegård J, Mortensen FV, Cronin-Fenton D. Chronic Pancreatitis and Pancreatic Cancer Risk: A Systematic Review and Meta-analysis. The American Journal of Gastroenterology. 2017; 112: 1366–1372. https://doi.org/10.1038/ajg.2017.218

[7] Wen A, Pan SY, Dadgar K, Yaghoobi M. Risk of Pancreatic Cancer and Precancerous Lesions in Patients With Chronic Pancreatitis: A Systematic Review and Meta-Analysis. Journal of Clinical Gastroenterology. 2025; 59: 820–832. https://doi.org/10.1097/MCG.0000000000002187

[8] Xuan M, Gu X, Li J, Huang D, Xue C, He Y. Polyamines: their significance for maintaining health and contributing to diseases. Cell Communication and Signaling : CCS. 2023; 21: 348. https://doi.org/10.1186/s12964-023-01373-0

[9] Ou Y, Wang SJ, Li D, Chu B, Gu W. Activation of SAT1 engages polyamine metabolism with p53-mediated ferroptotic responses. Proceedings of the National Academy of Sciences of the United States of America. 2016; 113: E6806–E6812. https://doi.org/10.1073/pnas.1607152113

[10] Madeo F, Eisenberg T, Pietrocola F, Kroemer G. Spermidine in health and disease. Science (New York, N.Y.). 2018; 359: eaan2788. https://doi.org/10.1126/science.aan2788

[11] Damiani E, Wallace HM. Polyamines and Cancer. Methods in Molecular Biology (Clifton, N.J.). 2018; 1694: 469–488. https://doi.org/10.1007/978-1-4939-7398-9_39

[12] Eisenberg T, Abdellatif M, Schroeder S, Primessnig U, Stekovic S, Pendl T, et al. Cardioprotection and lifespan extension by the natural polyamine spermidine. Nature Medicine. 2016; 22: 1428–1438. https://doi.org/10.1038/nm.4222

[13] Satarker S, Wilson J, Kolathur KK, Mudgal J, Lewis SA, Arora D, et al. Spermidine as an epigenetic regulator of autophagy in neurodegenerative disorders. European Journal of Pharmacology. 2024; 979: 176823. https://doi.org/10.1016/j.ejphar.2024.176823

[14] Asai Y, Itoi T, Sugimoto M, Sofuni A, Tsuchiya T, Tanaka R, et al. Elevated Polyamines in Saliva of Pancreatic Cancer. Cancers. 2018; 10: 43. https://doi.org/10.3390/cancers10020043

[15] Lee MS, Dennis C, Naqvi I, Dailey L, Lorzadeh A, Ye G, et al. Ornithine aminotransferase supports polyamine synthesis in pancreatic cancer. Nature. 2023; 616: 339–347. https://doi.org/10.1038/s41586-023-05891-2

[16] Soda K. Spermine and gene methylation: a mechanism of lifespan extension induced by polyamine-rich diet. Amino Acids. 2020; 52: 213–224. https://doi.org/10.1007/s00726-019-02733-2

[17] Hesterberg RS, Cleveland JL, Epling-Burnette PK. Role of Polyamines in Immune Cell Functions. Medical Sciences (Basel, Switzerland). 2018; 6: 22. https://doi.org/10.3390/medsci6010022

[18] Puleston DJ, Baixauli F, Sanin DE, Edwards-Hicks J, Villa M, Kabat AM, et al. Polyamine metabolism is a central determinant of helper T cell lineage fidelity. Cell. 2021; 184: 4186–4202.e20. https://doi.org/10.1016/j.cell.2021.06.007

[19] Gao C, Sheteiwy MS, Lin C, Guan Y, Ulhassan Z, Hu J. Spermidine Suppressed the Inhibitory Effects of Polyamines Inhibitors Combination in Maize (*Zea mays* L.) Seedlings under Chilling Stress. Plants (Basel, Switzerland). 2021; 10: 2421. https://doi.org/10.3390/plants10112421

[20] Kjellström J, Oredsson SM, Wennerberg J. Increased toxicity of a trinuclear Pt-compound in a human squamous carcinoma cell line by polyamine depletion. Cancer Cell International. 2012; 12: 20. https://doi.org/10.1186/1475-2867-12-20

[21] Rollins-Smith LA, Ruzzini AC, Fites JS, Reinert LK, Hall EM, Joosse BA, et al. Metabolites Involved in Immune Evasion by *Batrachochytrium dendrobatidis* Include the Polyamine Spermidine. Infection and Immunity. 2019; 87: e00035–19. https://doi.org/10.1128/IAI.00035-19

[22] Wang LJ, He L, Hao L, Guo HL, Zeng XP, Bi YW, et al. Isoliquiritigenin ameliorates caerulein-induced chronic pancreatitis by inhibiting the activation of PSCs and pancreatic infiltration of macrophages. Journal of cellular and molecular medicine. 2020; 24: 9667–9681. https://doi.org/10.1111/jcmm.15498

[23] Lin WR, Yen TH, Lim SN, Perng MD, Lin CY, Su MY, etal. Granulocyte colony-stimulating factor reduces fibrosis in a mouse model of chronic pancreatitis. PLoS One. 2014; 9: e116229. https://doi.org/10.1371/journal.pone.0116229

[24] Nakanishi S, Cleveland JL. Polyamine Homeostasis in Development and Disease. Medical Sciences (Basel, Switzerland). 2021; 9: 28. https://doi.org/10.3390/medsci9020028

[25] Murray-Stewart TR, Woster PM, Casero RA, Jr. Targeting polyamine metabolism for cancer therapy and prevention. The Biochemical Journal. 2016; 473: 2937–2953. https://doi.org/10.1042/BCJ20160383

[26] Fölsch UR, Löser C, Alves F. Polyamines in pancreatic growth. Digestion. 1990; 46: 345–351. https://doi.org/10.1159/000200407

[27] Uimari A, Merentie M, Sironen R, Pirnes-Karhu S, Peräniemi S, Alhonen L. Overexpression of spermidine/spermine N1-acetyltransferase or treatment with N1-N11-diethylnorspermine attenuates the severity of zinc-induced pancreatitis in mouse. Amino Acids. 2012; 42: 461–471. https://doi.org/10.1007/s00726-011-1025-9

[28] Räsänen TL, Alhonen L, Sinervirta R, Uimari A, Kaasinen K, Keinänen T, et al. Gossypol activates pancreatic polyamine catabolism in normal rats and induces acute pancreatitis in transgenic rats over-expressing spermidine/spermine N1-acetyltransferase. Scandinavian Journal of Gastroenterology. 2003; 38: 787–793. https://doi.org/10.1080/00365520310003273

[29] Fan YT, Yin GJ, Xiao WQ, Qiu L, Yu G, Hu YL, et al. Rosmarinic Acid Attenuates Sodium Taurocholate-Induced Acute Pancreatitis in Rats by Inhibiting Nuclear Factor-κB Activation. The American Journal of Chinese Medicine. 2015; 43: 1117–1135. https://doi.org/10.1142/S0192415X15500640

[30] Lv P, Li HY, Ji SS, Li W, Fan LJ. Thalidomide alleviates acute pancreatitis-associated lung injury via down-regulation of NFkB induced TNF-a. Pathology-Research and Practice. 2014; 210: 558–564. https://doi.org/10.1016/j.prp.2014.04.022

[31] Huang H, Liu Y, Daniluk J, Gaiser S, Chu J, Wang H, et al. Activation of nuclear factor-κB in acinar cells increases the severity of pancreatitis in mice. Gastroenterology. 2013; 144: 202–210. https://doi.org/10.1053/j.gastro.2012.09.059

[32] Alonso-Curbelo D, Ho YJ, Burdziak C, Maag JLV, Morris JP, 4th, Chandwani R, et al. A gene-environment-induced epigenetic program initiates tumorigenesis. Nature. 2021; 590: 642–648. https://doi.org/10.1038/s41586-020-03147-x

[33] Burdziak C, Alonso-Curbelo D, Walle T, Reyes J, Barriga FM, Haviv D, et al. Epigenetic plasticity cooperates with cell-cell interactions to direct pancreatic tumorigenesis. Science (New York, N.Y.). 2023; 380: eadd5327. https://doi.org/10.1126/science.add5327

[34] Lyko F. The DNA methyltransferase family: a versatile toolkit for epigenetic regulation. Nature Reviews. Genetics. 2018; 19: 81–92. https://doi.org/10.1038/nrg.2017.80

[35] Kang GH, Lee HJ, Hwang KS, Lee S, Kim JH, Kim JS. Aberrant CpG island hypermethylation of chronic gastritis, in relation to aging, gender, intestinal metaplasia, and chronic inflammation. The American Journal of Pathology. 2003; 163: 1551–1556. https://doi.org/10.1016/S0002-9440(10)63511-0

[36] Harbison RA, Pandey R, Considine M, Leone RD, Murray-Stewart T, Erbe R, et al. Interrogation of T Cell-Enriched Tumors Reveals Prognostic and Immunotherapeutic Implications of Polyamine Metabolism. Cancer Research Communications. 2022; 2: 639–652. https://doi.org/10.1158/2767-9764.crc-22-0061

[37] Travers M, Brown SM, Dunworth M, Holbert CE, Wiehagen KR, Bachman KE, et al. DFMO and 5-Azacytidine Increase M1 Macrophages in the Tumor Microenvironment of Murine Ovarian Cancer. Cancer Research. 2019; 79: 3445–3454. https://doi.org/10.1158/0008-5472.CAN-18-4018

[38] Tharp KM, Kersten K, Maller O, Timblin GA, Stashko C, Canale FP, et al. Tumor-associated macrophages restrict $CD8^{+}$ T cell function through collagen deposition and metabolic reprogramming of the breast cancer microenvironment. Nature Cancer. 2025; 5: 1045–1062. https://doi.org/10.1038/s43018-024-00775-4

[39] Guo T, Li B, Gu C, Chen X, Han M, Liu X, et al. PGC-1α inhibits polyamine metabolism in Cyclin E1-driven ovarian cancer. Cancer Medicine. 2019; 8: 7754–7761. https://doi.org/10.1002/cam4.2637

[40] Yang H, Zhang X, Zhang S, Yang Y, Chen Y, Jiang Y, et al. Targeting spermine metabolism to overcome immunotherapy resistance in pancreatic cancer. Nature Communications. 2025; 16: 7827. https://doi.org/10.1038/s41467-025-63146-2